A Contrast Adjustment Thresholding Method for Surface Defect Detection Based on Mesoscopy

Moe Win, *Student Member, IEEE*, A. R. Bushroa, M. A. Hassan, N. M. Hilman, *Student Member, IEEE*, and Ari Ide-Ektessabi

***Abstract*—Titanium-coated surfaces are prone to tiny defects such as very small cracks, which are not easily observable by the naked eye or optical microscopy. In this study, two new thresholding methods, namely contrast-adjusted Otsu's method and contrast-adjusted median-based Otsu's method, are proposed for automated defect detection system for titanium-coated aluminum surfaces. The two proposed methods were compared with four existing thresholding techniques in terms of accuracy and speed of defect detections for images of 700, 900, and 1000 dpi obtained using high-resolution scanning. Experimental results have shown that the proposed contrast-adjusting methods have performance similar to minimum error thresholding (MET) and are generally better than Otsu's method.**

***Index Terms*—Coated surface inspection, defect detection, high-resolution scanning, image analysis, image processing, mesoscopy.**

I. Introduction

INSPECTION and detection of defects on coated surfaces are essential steps in the preliminary assessment of coating processes. Defects that are identified can then be modified to satisfy predetermined quality requirements or in cases of severe defects, the coatings would be rejected. In addition, close inspection of physical abnormalities in the coating would provide an understanding into the possible mechanism of defects formation, and the knowledge gained can then be implemented into improvements of the coating process.

Several nondestructive techniques (NDTs) are available for detecting defects on coated surface. Common techniques employ the use of a fluorescent material on the coating layer. Defects can be located and measured based on the fluorescence emission [1].

Other techniques include mapping surface potentials using electrostatic methods [2], characterization of film failures by bismuth electrodeposition [3], and interfacial defects detection using infrared thermography [1], [4]. Although these methods can be used to detect defects in coating, they require specific procedures and set up, which may not be easily be integrated into the assembly lines for a production environment.

In a production environment, manufacturers usually adopt visual inspection techniques to detect product defects along the assembly or production line. These inspection methods use image processing and analysis to determine nonconformity of products based on predetermined criteria, and have been successfully used to detect surface defects on LCD screens [5], ceramic and tiles [6], steel [7]–[9], and textiles [10], [11]. Visual inspection techniques were also used to evaluate nonuniformity on surfaces of bottle caps [12] and detect defects on solar modules [13].

Image acquisition is an important process in visual inspection. Traditionally, optical microscopy is used for surface inspection to capture high-resolution images, although it has limited field of view and is more suitable for small samples [8]. In contrast, conventional photography can capture the subject as a whole due to its large field of view; however, the resolutions of the images obtained are much lower as compared to images from microscopy. A technique known as mesoscopy aims to combine the large field of view of traditional photography with the high-resolution capabilities of optical microscopy. Mesoscopic apparatus and techniques have been developed to capture large bulk volumes of materials. Past studies have used this technique to digitize cultural paintings [14], analyze textured patterns on Korean paper, and defect detection on LCD screens [15]. Mesoscopy have also been used with spectroscopic technique to reconstruct spectral reflectance of mineral pigments on Japanese paintings [16].

In manufacturing scenario, high-resolution image acquisition system has been used to detect defects on production samples, such as on steel surfaces as small as $2.75\,\mu\mathrm{m}$ per pixels [8]. These defects are usually miniscule in size, requiring a very high-resolution image of the surface for analysis. An important process in image analysis is thresholding, which reduces the color or grayscale image into binary. Thresholding is the simplest technique to segment an image into regions having common properties. It creates black and white binary images from grayscale or color images by transforming the intensity of

Manuscript received October 02, 2014; revised March 12, 2015; accepted March 22, 2015. Date of publication March 30, 2015; date of current version June 02, 2015. This work was supported in part by the Ministry of Higher Education with High Impact Research (HIR) under Grant UM.C/625/1/HIR/MOHE/ENG/27, and in part by Japan International Cooperation Agency (JICA) under the ASEAN University Network (AUN)/ Southeast Asia Engineering Education Development Network (SEED-Net) Collaborative Research with Industry (CRI) Program under Grant PG116-2013A and Grant RP017-2012A. Paper no. TII-15-0084.

M. Win, A. R. Bushroa, and N. M. Hilman are with the Center of Advanced Manufacturing and Material Processing (AMMP), Department of Mechanical Engineering, University of Malaya, 50603 Kuala Lumpur, Malaysia.

M. A. Hassan is with the Center of Advanced Manufacturing and Material Processing (AMMP), Department of Mechanical Engineering, University of Malaya, 50603 Kuala Lumpur, Malaysia, and also with the Mechanical Engineering Department, Faculty of Engineering, Assiut University, 71516 Assiut, Egypt (e-mail: mohsenegypt@um.edu.my).

A. Ide-Ektessabi is with the Advanced Imaging Laboratory, Graduate School of Engineering, Kyoto University Katsura Campus, 615-8540 Kyoto, Japan.

Color versions of one or more of the figures in this paper are available online at http://ieeexplore.ieee.org.

Digital Object Identifier 10.1109/TII.2015.2417676

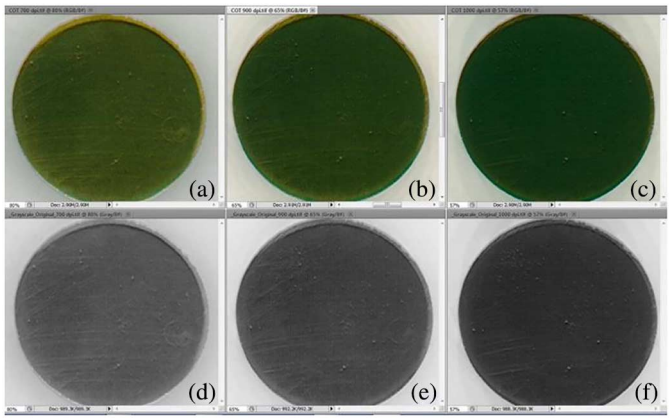

Fig. 1. (a) Original 700 dpi. (b) Original 900 dpi. (c) Original 1000 dpi. (d) Grayscale 700 dpi. (e) Grayscale 900 dpi. (f) Grayscale 1000 dpi.

all pixels to single values of either one or zero. Thresholding reduces the intensity of pixels below a certain value to zero (black), whereas pixels above the designated value are given one (white). Thresholding is useful for rapid evaluation on image segmentation due to its simplicity and fast processing speed.

Otsu's method of thresholding [17] is a popular technique for image thresholding and has been used as the default method for thresholding in software such as MATLAB. Kittler and Illingworth have developed a minimum error thresholding (MET) method [18], which has been proved to be superior to other methods of thresholding in a survey of 40 different methods [19]. Modified approaches using these methods were also proposed, in which the median of the image histogram data is used instead of the mean. The median extension of the original Otsu's method and MET were found to work better than their original counterpart for images with highly skewed and heavy-tailed color distribution [20].

In this paper, a contrast-adjusted Otsu's method and contrast-adjusted median-based Otsu's method were developed to distinguish coated and uncoated regions of metal specimens by applying image-specific contrast adjustments and then utilizing Otsu's method and median-based Otsu's method for the thresholding process. The thresholding will classify the segments in the image into coated and uncoated regions. The performance of the two proposed methods is then compared with Otsu's method, median-based Otsu's method, MET, and the median-based MET.

II. Methodology and Testing

A. Image Acquisition and Preparation

In this study, images of titanium-coated aluminum disk specimens are captured at high resolutions of 700, 900, and 1000 dpi using a line sensor camera of high-spatial accuracy and color fidelity. The image size was constrained to 1000×1000 pixels. Thus, one pixel is approximately equivalent to 36, 28, and 25 μm for 700, 900, and 1000 dpi resolutions, respectively. Fig. 1 shows the images of the sample captured at different resolutions and their respective grayscale image.

B. Image Thresholding and Binarization

For defect detection, the color image is first converted to grayscale and a thresholding technique is then utilized to obtain the corresponding black and white image. It is expected that the defect would be highlighted in a different color (white) as compared to the rest of the coating (black).

The grayscale image can be expressed in L gray levels $[1, 2, \ldots, L]$. The number of points with gray level at j is denoted by m_j and the entire number of points can be expressed as $M = m_1 + m_2 + \cdots + m_L$. The histogram of this gray level is regarded as an occurrence distribution of probability, which can be expressed as

$$p(k) = \frac{m_k}{M}, \quad p(k) \geq 0, \ \sum\nolimits_{k=1}^{L} p(k) = 1. \tag{1}$$

The threshold t is the gray level that divides the image into two classes: 1) C_0; and 2) C_1, i.e., foreground and background. The class C_0 represents pixels within levels $[1, 2, \ldots, t]$ and C_1 denotes pixels within level $[t + 1, \ldots, L]$.

1) Otsu's Method for Thresholding: The Otsu's method finds the optimum threshold $t*$ by maximizing the between-class variance [28]

$$t^* = \underset{1 \leq t \leq L}{\operatorname{argmax}}\, \sigma_B^2 \tag{2}$$

where the between-class variance σ_B^2 is given by

$$\sigma_B^2 = \omega_0(\mu_0 - \mu_t)^2 + \omega_1(\mu_1 - \mu_t)^2 \tag{3}$$

where the occurrence of probabilities of the two classes ω_o and ω_1, the average of the two classes μ_0 and μ_1, the total average μ_T, and the foreground and the background class variance σ_0^2 and σ_1^2 can be expressed, respectively, as

$$\omega_0(\mathrm{t}) = \sum_{\mathrm{k}=1}^{\mathrm{t}} p(k) \tag{4}$$

$$\omega_1(t) = 1 - \omega_0(t) = \sum_{k=t+1}^{L} p(k) \tag{5}$$

$$\mu_0(t) = \sum_{k=1}^{t} \frac{k.p(k)}{\omega_0(t)} = \frac{1}{\omega_0(t)} \sum_{k=1}^{t} k \,.\, p(k) \tag{6}$$

$$\mu_1(t) = \sum_{k=t+1}^{L} \frac{k.p(k)}{\omega_1(t)} = \frac{1}{1 - \omega_0(t)} \sum_{k=t+1}^{L} k \,.\, p(k) \tag{7}$$

$$\mu_T = \sum_{k=1}^{L} k \,.\, p(k) \tag{8}$$

$$\sigma_0^2(t) = \sum_{k=1}^{t} \left(k - \mu_0(k)\right)^2 .\, p(k) \tag{9}$$

$$\sigma_1^2(t) = \sum_{k=t+1}^{L} \left(k - \mu_1(k)\right)^2 .\, p(k) \tag{10}$$

$$\sigma_T^2 = \sum_{k=1}^{L} \left(k - \mu_T\right)^2 .\, p(k). \tag{11}$$

It was found that maximizing between-class variance σ_B^2 is similar to minimizing within-class variance σ_W^2 or the mean square error between the resultant binary image and the original grayscale image based on a simple relationship [20]

$$\sigma_B^2 + \sigma_W^2 = \sigma_T^2. \tag{12}$$

The within-class variance σ_w^2 is given by

$$\sigma_W^2 = \omega_0(t)\sigma_0^2 + \omega_1(t)\sigma_1^2. \tag{13}$$

Therefore, the threshold $t*$ can also be found by minimizing within-class variance

$$t* = \underset{1\le t\le L}{\operatorname{argmin}}\, \sigma_W^2 = \underset{1\le t\le L}{\operatorname{argmin}}\, \{\omega_0(t)\sigma_0^2 + \omega_1(t)\sigma_1^2\}. \tag{14}$$

2) Median-Based Extension of Otsu's Method: A median-based extension of the Otsu's thresholding method has been shown to be more robust in the determination of threshold, especially when the distribution is skewed and heavy-tailed [20]. In this study, the median-based Otsu's method is applied using median values instead of mean values of the grayscale-level distribution, and finding the mean absolute deviation (MAD) from the median to estimate the dispersion instead of the variance, as proposed by Xue and Titterington [20].

The threshold is selected by

$$t* = \underset{1\le t\le L}{\operatorname{argmin}}\{\omega_0\, \mathrm{MAD}_0\,(t) + \omega_1\, \mathrm{MAD}_1\,(t)\} \tag{15}$$

where MAD_0 and MAD_1 are the MADs from the median for the foreground and background classes C_0 and C_1 giving

$$\mathrm{MAD}_0(t) = \sum_{k=1}^{t} \frac{p(k)}{\omega_0(t)} |k - m_1(t)| \tag{16}$$

$$\mathrm{MAD}_1(t) = \sum_{k=t+1}^{L} \frac{p(k)}{\omega_1(t)} |k - m_2(t)| \tag{17}$$

where m_1 and m_2 are the sample median for C_0 and C_1, respectively.

3) MET Method: Another method for determining the threshold is the Kittler and Illingworth's MET [18]. This method optimizes the average pixel classification error rate directly and has been found to be the best thresholding technique for NDT images [19].

The threshold is selected by

$$t* = \underset{1\le t\le L}{\operatorname{argmin}} \left\{ \omega_0(t) \log \frac{\sigma_0(t)}{\omega_0(t)} + \omega_1(t) \log \frac{\sigma_1(t)}{\omega_1(t)} \right\}. \tag{18}$$

4) Median-Based Extension of MET Method: Similar to Otsu's method, the median-based MET is regarded to be more robust in finding the optimum threshold in the presence of skew and heavy tail in the gray-level distribution [20]. Thus, for this study, the median-based MET, as proposed by Xue and Titterington [20], was utilized. The threshold for median-based MET is selected using similar set of rule for finding the optimum threshold using MET, substituting the standard deviation of a particular class with the MAD from the class median

$$t* = \underset{1\le t\le L}{\operatorname{argmin}} \left\{ \omega_0(t) \log \frac{\mathrm{MAD}_0(t)}{\omega_0(t)} + \omega_1(t) \log \frac{\mathrm{MAD}_1(t)}{\omega_1(t)} \right\}. \tag{19}$$

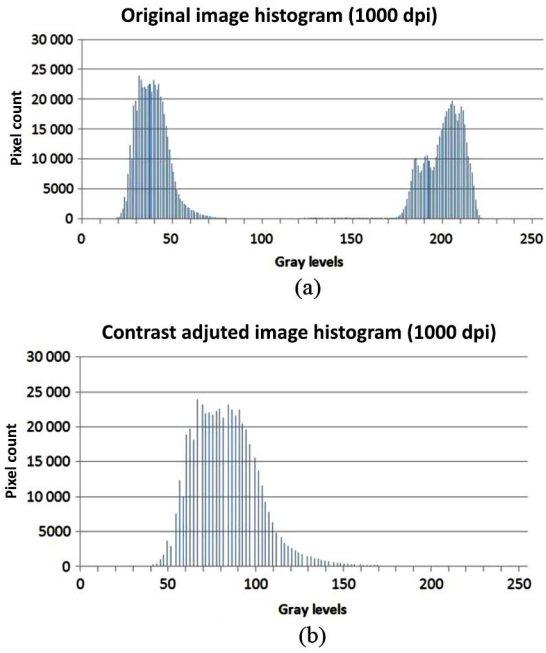

Fig. 2. (a) Original image histogram. (b) Histogram of an image that has undergone contrast adjustment subroutine with the background removed.

C. Proposed Thresholding Methods

1) Contrast-Adjusted Otsu's Method: In this study, a thresholding method is proposed that includes a contrast adjustment routine utilizing Otsu's thresholding (14) to calculate the maximum cutoff value for image contrast stretching, and then to apply the same Otsu's thresholding method to calculate the threshold of the contrast-enhanced grayscale image for conversion to a black and white image.

As Otsu's method calculates the threshold to divide the image into two classes according to the gray levels, using the threshold value as the maximum cutoff value for image contrast stretching yields a unimodal histogram, as shown in Fig. 2(b), indicating that the image is uniform. The contrast adjustment was made by mapping the foreground class $[1,\ 2, \ldots, t]$ to the original range of the image $[1,\ 2, \ldots, L]$. This can be expressed in pseudocode as follows:

```
...
GrayscaleImage I [image.rows, image.columns];
MaximumGrayLevel L = 255;

Threshold t = Otsu_Method(I); //from Equation 14

for r = 1:image.rows
   for c = 1:image.columns
      I [r, c] = (I [r, c] / t) * L;
   end
end
...
```

The resultant image is then converted to a binary representation, utilizing the threshold value calculated by Otsu's method (14). As Otsu's method assumes that the image histogram is bimodal, applying it on the contrast-enhanced image will split the unimodal distribution into two [18]. This characteristic

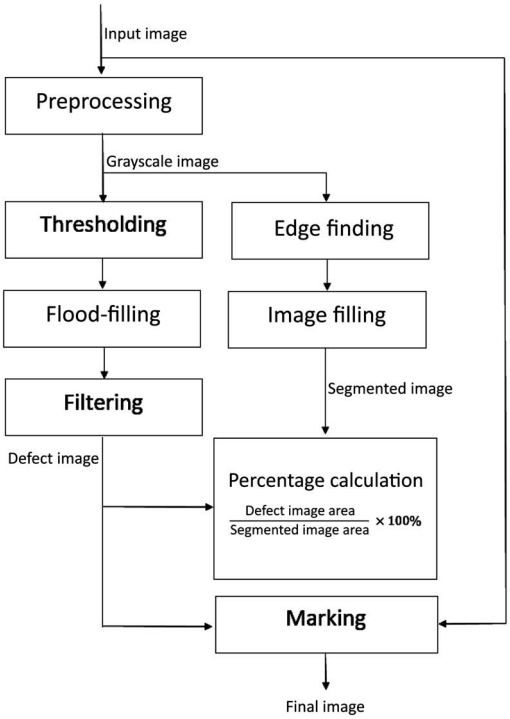

Fig. 3. Flow diagram of the image processing and analysis.

enables the contrast-adjusted method to be more accurate, as the defects on the coated material are categorized along with the background of the image resulting to a simpler image for segmentation.

2) Contrast-Adjusted Median-Based Otsu Method: Similarly, for the second proposed method, the contrast adjustment is made by mapping the foreground class to the original range of the image as described in the pseudocode. Equation (15) is used to determine the threshold, as described in median-based Otsu's method. This approach is not applicable to the MET method and its median-based extension, as the criterion for MET will fail to find any local minima to compute the optimum threshold as the distribution has only one mode.

Utilizations of the thresholding methods are incorporated in the steps for processing and analyzing the image, as shown in Fig. 3. These six different methods convert the grayscale images into their respective binary representation (black and white). In a binary image, a pixel has either the value of 1 (white) or 0 (black). The pixels are converted to 1 if their gray levels are $> t*$ and are converted to 0 if the gray levels $\leq t*$. Since the coating is assumed to be uniform, binarization will completely represent coated surface to black. Defects will be highlighted since their pixels representation will be converted to 1 (white) in the binarization process.

D. Defect Detection and Analysis

1) Defect Filtering and Recording: After binarization, the area containing defects is distinguishable, as the defects will have the same pixel values as the white background. A flood-fill algorithm [21] is used to find connected components with eight-connected neighborhood. The connected components are then selected according to its size A_k based on a predetermined minimum size $i_{\min}$ and maximum size $i_{\max}$ value to account for noises and effects of uneven light source

$$i_{\min} < A_k < i_{\max}. \tag{20}$$

The value of $i_{\min}$ is set at 2, whereas $i_{\max}$ is set at 500 for the 700 and 900 dpi images. This configuration indicates that the smallest defect detectable is 3 pixels wide, which is approximately $100\,\mu\mathrm{m}$ for 700 dpi and $85\,\mu\mathrm{m}$ for 900 dpi. For the 1000 dpi image, the $i_{\min}$ is set at 3, indicating the smallest defect detection resolution of 4 pixels, equivalent to $100\,\mu\mathrm{m}$.

The area of each defects is also calculated. The area of one defect is expressed as A_k, where $k = 1, 2, \ldots, N$, and N is the number of defects detected based on the number of connected components that agree with the set of required conditions (20). For each A_k, the area is calculated based on the number of pixels m for the corresponding area of defects A_k, such that $A_k = a_1 + a_2 + \cdots + a_m$.

The centroid of the defects can be expressed as $C_k\ (x,\ y)$, where $k = 1,\ 2, \ldots, N$, and N is the number of the defects detected based on the number of connected components that agree with the condition set in A. Each C_k is calculated based on the centroid of pixels m for the corresponding area of defects A_k. The centroid of the defect can be calculated using

$$C_{kx} = \frac{\sum c_{mx} a_m}{A_k}, \quad C_{ky} = \frac{\sum c_{my} a_m}{A_k} \tag{21}$$

where C_{kx} is the x-coordinate and C_{ky} is the y-coordinate of the defects.

The centroid value indicates the position of the defects. In this study, we mark the location of defects in the original image by red crosses having the size of 3 pixels. Since the processed image and the original image have the same sizes, the position of the defects in the original image directly correlates with the binary image.

2) Sample Surface Area Estimation: The surface area is calculated to determine the area of defects with respect to the coated sample surface area. In this study, an image segmentation technique is used for edge determination using the Sobel operator [22]. The edge detection was applied on the grayscale image, which resulted in a binary gradient mask that exhibited a stark contrast between the sample and the background, which can then be segmented effectively. The surface area of the coated samples was computed based on the filled binary gradient mask, as it represents the surface of the sample given by A_T.

3) Calculation of Defect Percentage: The percentage of the sum of defect area as compared to the total size of the samples is calculated to determine the extent of defects detectable using the methods proposed. The total defect surface area A_D is represented by the summation of surface areas of A_k for N number of detected defects, denoted as

$$A_D = A_1 + A_2 + \cdots + A_N = \sum_{k=1}^{N} A_k. \tag{22}$$

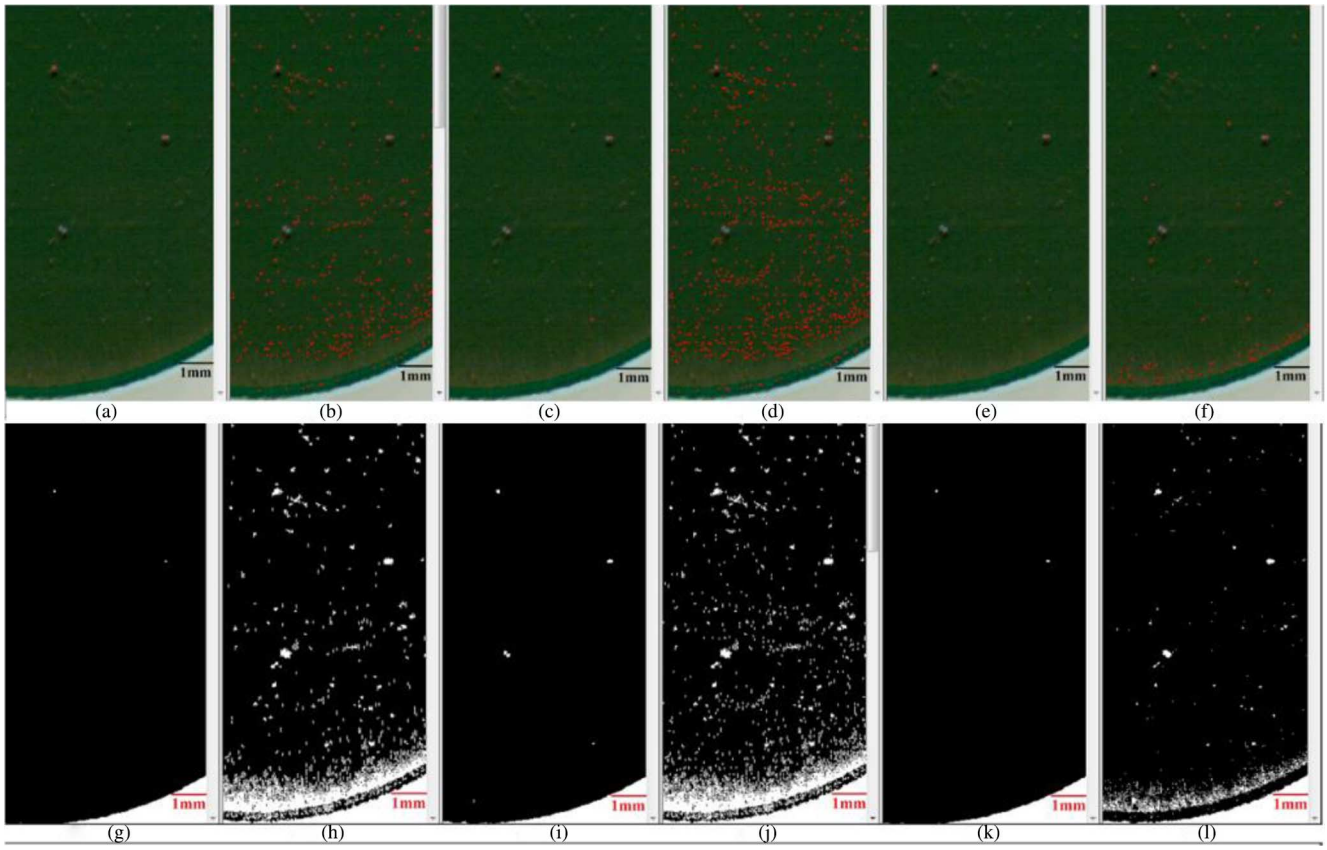

Fig. 4. Defect detection results from (a) Otsu's method; (b) Median-based Otsu; (c) Contrast-adjusted Otsu; (d) Median-based contrast adjusted Otsu; (e) MET; and (f) Median-based MET and the corresponding filtered binary representation containing defects under it. (g) Otsu. (h) Median-based Otsu. (i) Contrast-adjusted Otsu. (j) Median-based contrast adjusted Otsu. (k) MET. (l) Median-based MET. The red crosses indicate position of the defects that matches the defects (white) position in the filtered binary images. All the images are from 1000 dpi results.

TABLE I
GRAY-LEVEL THRESHOLD AND DEFECT DETECTION FOR 700 DPI IMAGE

No.	THRESHOLDING METHOD	GREY-LEVEL THRESHOLD t^*	NUMBER OF DEFECTS DETECTED	TOTAL DEFECT SURFACE AREA (PIXELS)	PERCENTAGE OF DEFECTS (%)	TIME TAKEN (S)
1	Otsu's method [17]	0.5216	4	24	0.0092	1.23
2	Median-based Otsu [20]	0.5098	2	6	0.0023	56.64
3	Otsu's method—Contrast Adjustment (proposed)	0.7216	12	102	0.0410	1.69
4	Median-based Otsu—Contrast adjustment (proposed)	0.7137	19	104	0.0418	55.97
5	MET [18]	0.5882	5	27	0.0103	1.18
6	Median-based MET [20]	0.5333	3	11	0.0027	74.58

TABLE II
GRAY-LEVEL THRESHOLD AND DEFECT DETECTION FOR 900 DPI IMAGE

No.	THRESHOLDING METHOD	GREY-LEVEL THRESHOLD t^*	NUMBER OF DEFECTS DETECTED	TOTAL DEFECT SURFACE AREA (PIXELS)	PERCENTAGE OF DEFECTS (%)	TIME TAKEN (S)
1	Otsu's method [17]	0.5137	1	8	0.0020	1.89
2	Median-based Otsu [20]	0.4863	1	16	0.0040	56.61
3	Otsu's method—contrast Adjustment (proposed)	0.6863	35	517	0.1309	1.75
4	Median-based Otsu—contrast adjustment (proposed)	0.6784	38	520	0.1317	56.34
5	MET (18)	0.5137	1	8	0.0020	1.28
6	Median-based MET [20]	0.3961	16	132	0.0327	56.78

TABLE III
GRAY-LEVEL THRESHOLD AND DEFECT DETECTION FOR 1000 DPI IMAGE

No.	THRESHOLDING METHOD	GREY-LEVEL THRESHOLD t^*	NUMBER OF DEFECTS DETECTED	TOTAL DEFECT SURFACE AREA (PIXELS)	PERCENTAGE OF DEFECTS (%)	TIME TAKEN (S)
1	Otsu's method [17]	0.4667	2	9	0.0017	1.92
2	Median-based Otsu [20]	0.1765	2275	19 244	3.6056	58.58
3	Otsu's method—contrast adjustment (proposed)	0.6549	10	109	0.0208	1.94
4	Median-based Otsu—contrast adjustment (proposed)	0.3765	2275	19 244	3.6056	59.03
5	MET [18]	0.4157	3	28	0.0052	1.28
6	Median-based MET [20]	0.2157	373	6212	1.1639	56.44

Thus, the percentage of defect P_d for each image can be calculated by

$$P_d = \frac{\sum_{k=1}^{N} A_k}{A_T} \times 100\%. \quad (23)$$

III. EXPERIMENT AND RESULTS

In the experiments, the proposed method is implemented in MATLAB R2013a and ran on an Intel Core i7-3770 CPU 3.40 GHz processor with a 16-GB RAM and a Windows 7 platform. The images obtained from the mesoscopic image capture system were processed in accordance to the steps shown in Fig. 4. Comparisons were made between the six thresholding methods on their ability and efficiency in detecting defects in the coated sample.

Table I shows the threshold level obtained from the image using the six thresholding methods, the total number of defects, the percentage of defects, and the total time taken to complete the detection tasks for 700 dpi images. Similarly, Tables II and III show the summary of results for 900 and 1000 dpi images, respectively. Generally, it was observed that higher resolution images yield the largest number of defects. The median-based methods generally detected more defects than their nonmedian counterparts, except for the case of applying median-based MET on the 700 dpi image. However, this high defect detection ability required more time to complete, as the data would need to be rearranged to obtain the median value. It can also be observed that for the cases of both contrast-adjusted and original Otsu's methods, higher resolution does not always indicate higher count of defects. Fig. 4 shows a segment of the results from the samples using 6 different algorithms for 1000 dpi resolution.

IV. DISCUSSIONS

To verify the accuracy of defect detection, the results were compared with images obtained using optical microscopy. Three regions on the sample that contains large defects were identified using a light optical microscope and were compared alongside their corresponding images obtained at 700, 900, and 1000 dpi. These regions, denoted as A, B, and C as shown in Figs. 5–7, were chosen for having defects larger than $50\ \mu\text{m}$. It can be shown that as the resolution of the image is increased, the defects are increasingly visible.

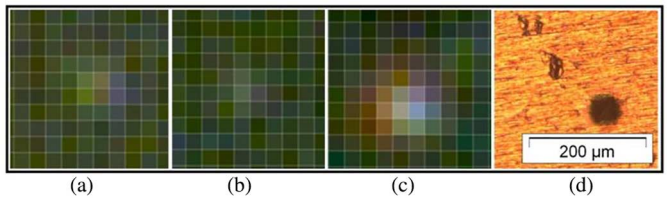

Fig. 5. Region A at (a) 700 dpi, (b) 900 dpi, (c) 1000 dpi, and (d) under microscope at 50× magnification.

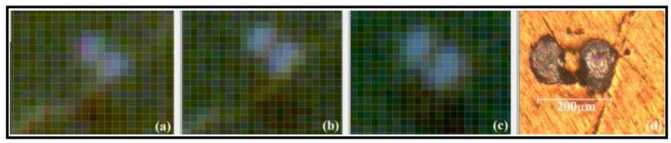

Fig. 6. Region B at (a) 700 dpi, (b) 900 dpi, (c) 1000 dpi, and (d) optical microscope at 50× magnification.

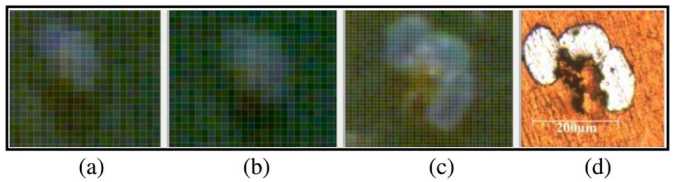

Fig. 7. Region C at (a) 700 dpi, (b) 900 dpi, (c) 1000 dpi, and (d) optical microscope at 50× magnification.

The three regions were also used to compare the accuracy and speed of the six thresholding methods in detecting defects. Fig. 8 summarized the comparison and the results. The methods have been arranged to rank the methods according to its ability to detect both region in the shortest time.

Since median-based methods involved determination of the median, thresholding methods of median-based Otsu, contrast-adjusted median-based Otsu, and median-based MET were found to take the longest times for defect detections. For low-resolution images, the computation time would not be apparent; however, for high-resolution images, the difference in efficiency would be noticeable. The computation can be improved by prearrangement of the intensity values prior to calculation of the means [20]. Furthermore, median-based methods had lower threshold values, which may increase the rate of false detection.

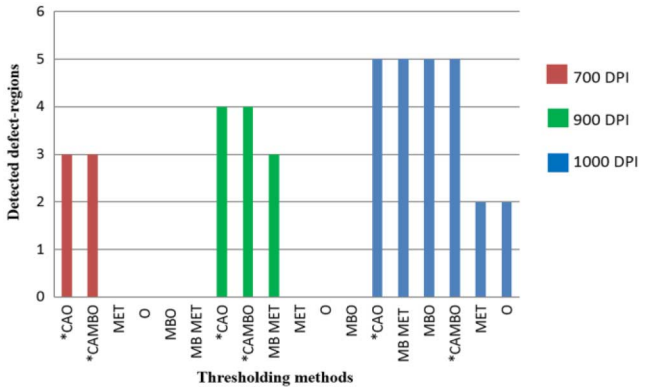

Fig. 8. Ranking of methods according to accuracy and speed. Faster and more accurate from left to right, categorized within similar image resolution. O, Otsu; MBO, median-based Otsu; CAO, contrast-adjusted Otsu; CAMBO, contrast-adjusted median-based Otsu; MET, minimum error thresholding; MBMET, median-based MET.

Such occurrence may be due to effects of lighting and shadows in the samples. As can be seen in Fig. 4, the effect of shadows in the lower region of the samples is identified as defects by the median-based thresholding methods.

The contrast-adjusted methods proposed in this study shows consistent defect detection performance for the three image resolutions of 700, 900, and 1000 dpi. Both contrast-adjusted Otsu and median-based Otsu detected the highest number of defects as compared to the other thresholding methods in the same category. This suggests that the contrast-adjusted method can be a useful complimentary method to threshold images with bimodal gray-level distribution. The method is similar in its efficiency as compared to MET, and is generally better than the Otsu's method currently employed in software packages such as MATLAB.

V. Conclusion and Future Works

Two thresholding methods, contrast-adjusted Otsu's method and contrast-adjusted median-based Otsu's method, were developed for the detection of defects on high-resolution images of titanium-coated aluminum specimens. The performance of the two methods was compared to four existing thresholding methods. It was found that the proposed methods were able to correctly detect the highest number of predetermined defects in different sets of image resolution and performed better than MET and Otsu's method. However, the lighting and shadow effects were found to influence the accuracy of defect detection. Thus, it is recommended that a *fuzzy clustering algorithm* or *wavelet analysis* is incorporated into the image preprocessing to distinguish affected regions and reduce false detections.

References

[1] R. Ebner, B. Kubicek, and G. Újvári, "Non-destructive techniques for quality control of PV modules: Infrared thermography, electro-and photoluminescence imaging," in *Proc. 39th Annu. Conf. IEEE Ind. Electron. Soc. (IECON'13)*, 2013, pp. 8104–8109.

[2] L. Vieira *et al*., "Scratch testing for micro- and nanoscale evaluation of tribocharging in DLC films containing silver nanoparticles using AFM and KPFM techniques," *Surf. Coat. Technol*., vol. 260, pp. 205–213, 2014.

[3] S. Holvoet *et al*., "Characterization of film failures by bismuth electrodeposition—Application to thin deformed fluorocarbon films for stent applications," *Electrochimica Acta*, vol. 55, no. 3, pp. 1042–1050, 2010.

[4] C. Meola and G. M. Carlomagno, "Infrared thermography to evaluate impact damage in glass/epoxy with manufacturing defects," *Int. J. Impact Eng*., vol. 67, pp. 1–11, 2014.

[5] T.-Y. Li *et al*., "Pretest gap mura on TFT LCDs using the optical interference pattern sensing method and neural network classification," *IEEE Trans. Ind. Electron*., vol. 60, no. 9, pp. 3976–3982, Sep. 2013.

[6] M. H. Karimi and D. Asemani, "Surface defect detection in tiling industries using digital image processing methods: Analysis and evaluation," *ISA Trans*., vol. 53, no. 3, pp. 834–844, 2014.

[7] Y. J. Jeon *et al*., "Defect detection for corner cracks in steel billets using a wavelet reconstruction method," *J. Opt. Soc. Amer. A Opt. Image Sci. Vis*., vol. 31, no. 2, pp. 227–237, 2014.

[8] C. Buck *et al*., "Rapid inclusion and defect detection system for large steel volumes," *ISIJ Int*., vol. 53, no. 11, pp. 1927–1935, 2013.

[9] W.-b. Li, C.-h. Lu, and J.-c. Zhang, "A lower envelope Weber contrast detection algorithm for steel bar surface pit defects," *Opt. Laser Technol*., vol. 45, pp. 654–659, 2013.

[10] J. A. Fernandez *et al*., "Fabric defect detection using the wavelet transform in an ARM processor," in *Proc. Image Process. Mach. Vis. Appl. V*, 2012, vol. 8300, p. 83000N.

[11] A. S. Nateri, F. Ebrahimi, and N. Sadeghzade, "Evaluation of yarn defects by image processing technique," *Optik Int. J. Light Electron Opt*., vol. 125, no. 20, pp. 5998–6002, 2014.

[12] W. J. Zhou *et al*., "A sparse representation based fast detection method for surface defect detection of bottle caps," *Neurocomputing*, vol. 123, pp. 406–414, 2014.

[13] D.-M. Tsai, S.-C. Wu, and W.-Y. Chiu, "Defect detection in solar modules using ICA basis images," *IEEE Trans. Ind. Informat*., vol. 9, no. 1, pp. 122–131, Feb. 2013.

[14] J. Kaneko *et al*., "Non-destructive analytical imaging of metallic surfaces using spectral measurements and ultrahigh-resolution scanning for cultural heritage investigation," in *Proc. IS&T/SPIE Electron. Imag*., 2012, p. 82911E.

[15] A. Ide-Ektessabi, J. A. Toque, and Y. Murayama, "Mesoscopy: A new approach for industrial in-line inspection," in *Proc. 4th Reg. Conf. Manuf*., November 9–10, 2011.

[16] J. A. Toque *et al*., "High-resolution multispectral scanning for mesoscopic investigation of discoloration of traditional Japanese pigments," in *Computational Color Imaging*. New York, NY, USA: Springer, 2015, pp. 195–207.

[17] N. Otsu, "A threshold selection method from gray-level histograms," *Automatica*, vol. 11, no. 285–296, pp. 23–27, 1975.

[18] J. Kittler and J. Illingworth, "Minimum error thresholding," *Pattern Recognit*., vol. 19, no. 1, pp. 41–47, 1986.

[19] M. Sezgin, "Survey over image thresholding techniques and quantitative performance evaluation," *J. Electron. Imag*., vol. 13, no. 1, pp. 146–168, 2004.

[20] J. H. Xue and D. M. Titterington, "Median-based image thresholding," *Image Vis. Comput*., vol. 29, no. 9, pp. 631–637, 2011.

[21] K. P. Fishkin and B. A. Barsky, "A family of new algorithms for soft filling," *SIGGRAPH Comput. Graph*., vol. 18, no. 3, pp. 235–244, 1984.

[22] P. Danielsson and O. Seger, "Generalized and separable Sobel operators," in *Machine Vision for Three-Dimensional Scenes*. San Diego, CA, USA: Academic, 1990, pp. 347–379.

Moe Win (S'15) received the B.Sc. degree (Hons.) in chemistry from Taungoo University (affiliated with Yangon University), Taungoo, Myanmar, in 2006, and the M.Sc. degree in chemical engineering from the Department of Technology of Isotopes and Hydrogen Energy, Mendeleyev University of Chemical Technology of Russia (MUCTR), Moscow, Russia, in 2011. He is currently pursuing the Ph.D. degree from the Department of Mechanical Engineering, Faculty of Engineering, University of Malaya, Kuala Lumpur, Malaysia.

Since 2007, he has been working as a Demonstrator with the Department of Chemistry, Taungoo University and Yangon University. He was a Research Fellow with the Advanced Imaging Laboratory, Kyoto University, Kyoto, Japan, in 2014. His research interests include mesoscopic inspection for industrial applications, surface engineering, and high-resolution image processing.

A. R. Bushroa received the Postgraduate degree in surface engineering from the University of Malaya (UM), Kuala Lumpur, Malaysia, in 2012.

She has been a Lecturer since 2004. In 2009, she went for a HLCB Ph.D. study leave scheme sponsored by the Ministry of Education, Malaysia. Her active role in teaching, research, management, and consultation rewarded her a Chartered Engineer (i.e., C.Eng.) by the Institution of Engineering and Technology (IET), Oxford, U.K., in 2012. Just after the Ph.D. graduation, she was appointed a Senior Lecturer with the Department of Engineering Design and Manufacture, Faculty of Engineering, which has now merged into the Department of Mechanical Engineering. At the same time, she has been an active member in the Advance Manufacturing and Material Processing (AMMP) Centre, University of Malaya, and is now establishing her research in surface engineering related studies locally and internationally.

M. A. Hassan received the Graduate degree in mechanical engineering from Minia University, Minya, Egypt, in 1991; Master's degree in mechanical engineering from Assiut University, Assiut, Egypt, in 1997; and the Ph.D. degree in information and production science (forming technology) from the Kyoto Institute of Technology, Kyoto, Japan, in 2002.

He is a Professor with the Department of Mechanical Engineering, Assiut University, Asyut, Egypt. He is currently a Visiting Associate Professor with the Department of Mechanical Engineering, Faculty of Engineering, University of Malaya, Kuala Lumpur, Malaysia. He has authored more than 40 research articles in the field of forming and microforming, microelectromechanical systems, piezoelectric thin films, and heart mechanics.

Dr. Hassan is a Registered Professional Engineer with the Board of Engineers of Egypt; a member of IMechE, U.K.; a member of the of the Japan Society for Technology of Plasticity; and a member of the Egyptian Nanotechnology Club. He was awarded the Ph.D. scholarship by the Japanese government in 1998.

N. M. Hilman (S'15) received the B.Eng. degree in computer-aided design and manufacturing engineering, and the M.Eng.Sc. degree in mechanical engineering (mechanical systems) from the University of Malaya, Kuala Lumpur, Malaysia, in 2009 and 2013, respectively.

He was with the Faculty of Engineering, University of Malaya, from 2009 to 2012. He was as Research Student with the Hagiwara Laboratory, Tokyo Institute of Technology, Meguro, Japan, in 2011. He is currently a Ph.D. candidate and Research Assistant at the Centre of Advanced Manufacturing and Material Processing (AMMP), University of Malaya, Kuala Lumpur, Malaysia. His research interests include image processing and analysis, high-resolution scanning and its industrial applications, and mechanical systems.

Ari Ide-Ektessabi received the Ph.D. degree in electronics engineering from the Faculty of Electronics Engineering, Kyoto University, Kyoto, Japan, in 1983.

He joined Kyoto University as an Associate Professor in 1991 and has been a Professor since 2001. He was the pioneer and leader of six major projects related to the application of advanced imaging technology in Japan. He has authored more than 300 papers in the field of analytical imaging in material science and engineering. His laboratory supervises and supports about ten laboratories in Japan, Asia, Europe, and Africa. His research interests include designing systems of charged particle beams, vacuum systems for fabrication and analysis of surfaces and materials, and analytical Imaging.